

Application of an RBF blending interpolation method to problems with shocks

Michael Harris¹, Alain Kassab¹, Eduardo Divo²

¹ *Mechanical and Aerospace Engineering Department*

University of Central Florida

4000 Central Florida Blvd., Orlando, FL, 32816, USA

e-mail: michael.f.harris@knights.ucf.edu, alain.kassab@ucf.edu

² *Department of Mechanical Engineering*

Embry-Riddle Aeronautical University

Daytona Beach, FL, USA

e-mail: divoe@erau.edu

Radial basis functions (RBF) have become an area of research in recent years, especially in the use of solving partial differential equations (PDE). Radial basis functions have an impressive capability in interpolating scattered data, even for data with discontinuities. Although, for infinitely smooth radial basis functions such as the multi-quadrics and inverse multi-quadrics, the shape parameter must be chosen properly to obtain accurate approximations while avoiding ill-conditioning of the interpolating matrices. The optimum shape parameter can vary depending on the field, such as in locations of sharp gradients or shocks. Typically, the shape parameter is chosen to maintain a high conditioning number for the interpolation matrix, rendering the RBF smooth [1–10]. However, this strategy fails for a problem with a shock or sharp discontinuity. Instead, in such cases the conditioning number must be kept small. The focus of this work is then to demonstrate the use of RBF interpolation in the approximation of sharp gradients or shocks by use of a RBF blending interpolation approach. This RBF blending interpolation approach is used to maintain the optimum shape parameter depending on the field. The approach is able to sense gradients or shocks in the field and adjust the shape parameter accordingly to keep excellent accuracy. Presented in this work, is an explanation of the RBF blending interpolation methodology and testing of the RBF blending interpolation approach by solving the Burger's equation using the virtual finite difference method.

Keywords: meshless methods, radial basis functions, multiquadrics, shape parameter, shocks.

1. INTRODUCTION

In engineering and sciences, most problems are governed by partial differential equations (PDE). There are solutions to special cases of partial differential equations, but for coupled non-linear PDE with complex geometry, the governing equations must be solved numerically. Mesh based numerical methods, such as Finite Difference Method (FDM), Finite Element Method (FEM), and Finite Volume Method (FVM) have been well developed and are the methods used today for solving partial differential equations [2–10]. These methods require connectivity to be defined within the domain allowing for the governing partial differential equations to be discretized and solved. The connectivity between points develops a mesh which must be predetermined before attempting a solution. The quality of the mesh can have an effect on convergence as well. The development of a high quality mesh that has both the resolution to capture the physics while also minimizing the number of points or cells, and thus minimizing computational time, can be an exhausting iterative process. For problems with complex geometry and physics, one could conclude this task to be impossible and must add simplifying assumptions or accept the solution. The

advancement of automated mesh generators sought to alleviate this process. However, the user is required to estimate, generate a mesh and inquire if the mesh has met an acceptable criterion. In other words, users must remain vigilant with respect to their inspection of automated meshes. Automated generators do not necessarily guarantee a good mesh and are far from being fully automated requiring significant amounts of time from the user [2–10].

In recent years, meshless methods have been an area of research and development. These techniques originate from spectral methods based on Legendre or Chebyshev polynomials, which require uniform point distribution [8–10]. The meshless techniques using radial basis functions (RBF) as the interpolation function, however, can be used on non-uniform distributions of points. The radial basis functions are based on the Euclidean distance and functions such as the Hardy multiquadrics and inverse multiquadrics, shown with other RBF in Fig. 1, are dependent on the shape parameter, c . These RBF meshless methods depend on local or global interpolation on irregular spatial distribution and not connectivity of points offering a solution to the complexity of mesh generation. The absence of the connection between points is how meshless methods facilitates the solution process, without the need to develop a mesh only requiring a point cloud and boundary nodes to solve.

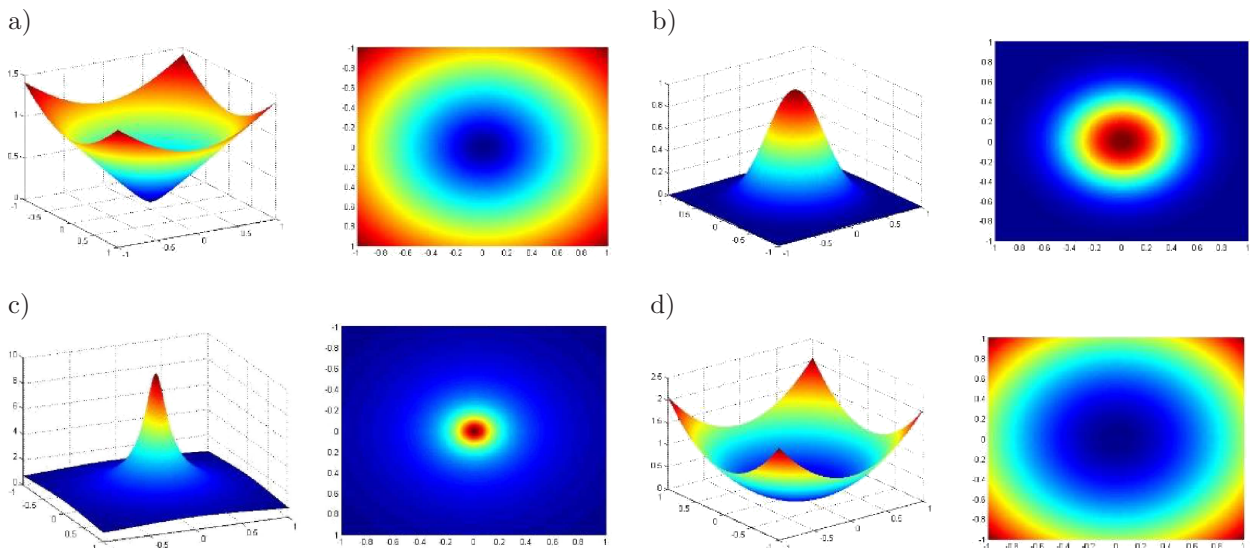


Fig. 1. Examples of radial basis functions: a) multiquadrics, b) Gaussian, c) inverse multiquadrics, d) thin plate spline.

There are many meshless methods in literature, but the focus of this work involves methods using radial basis function (RBF) interpolation. RBF interpolation has proven to give spectral accuracy, but while using the multiquadrics and inverse multiquadrics, the accuracy is dependent upon the shape parameter, c . The shape parameter is arbitrarily chosen or numerical experimentation is done to determine the best value. Typically, a higher valued shape parameter reduces error and the best value tends to be when the interpolation matrix is close to ill-conditioned [1, 2]. The ill-conditioning of the interpolation matrix does not allow for a global interpolation as solutions are not accurate due to ill-conditioning, but researchers have found that locally interpolating using RBF methods resolves these issues [2–4, 7, 8, 10].

The shape parameter being a value where the condition number of the interpolation matrix is large allows for convergence for smooth functions [1–10]. Typically, the shape parameter value needed for this case is arbitrarily large and this shape parameter which gives convergence is chosen throughout the solution [2]. In the presence of steep gradients or highly convective flows, this is not the case. Oscillations tend to appear using this approach of large shape parameter RBF interpolation. It can be determined that a low shape parameter value causing the conditioning number of interpolation matrix to be small provides better accuracy. So if one must solve regions

where the gradients are smooth while a steep gradient or discontinuity may exist downstream, the RBF interpolation schemes need to blend between high and low shape parameter values.

The use of RBF interpolation is typically used to solve for the derivatives directly. When dealing with highly convective fields or steep gradients, using RBF interpolation to solve for the derivatives directly can be difficult. This is due to the very little control of how information is past to the data center [4]. Another method will be used to test the blending approach called the RBF virtual point finite difference. This method uses the accuracy of the RBF interpolation to approximate the field variables in the domain at any point allowing for a finite difference stencil to be created. The creation of a stencil allows for the well-developed finite difference methods of today to be used.

In this work, the RBF interpolation of smooth and steep gradient functions are discussed showing how the shape parameter can change the accuracy. The formulation of the blended approach is described showing the approach taken to sense steep gradients and then switch from high conditioning to low conditioning and how well the RBF interpolation is capable of capturing the discontinuity. Finally, examples of solutions applying this approach are presented using the inviscid Burgers' equation as a model.

2. RBF INTERPOLATION OVERVIEW

The radial basis function interpolation is performed by assuming the solution to the functions is equal to the summation described by

$$f(x) = \sum_{j=1}^N \alpha_j \Psi_j(x), \quad (1)$$

where α_j is the weight or influence of node j and $\Psi_j(x)$ is the radial basis function. If the Hardy multiquadrics is chosen as the interpolation function, then $\Psi_j(x)$ is of the form

$$\Psi_j(x) = \sqrt{(x - x_j)^2 + c^2}, \quad (2)$$

where x is location of the node, x_j is a node surrounding x and c is the shape parameter. To find the weighting coefficients α_j , a system of equations can be formed describing the influence each node has on one another.

$$\Psi_j(x_i) = \sqrt{(x_i - x_j)^2 + c^2}, \quad (3)$$

$$f(x_i) = \sum_{j=1}^N \alpha_j \Psi_j(x_i). \quad (4)$$

We have the following the system of equations

$$[\Psi] \{\alpha\} = \{f\}. \quad (5)$$

Solving for $\{f\}$ we can find the

$$\{\alpha\} = [\Psi]^{-1} \{f\}. \quad (6)$$

Once the weighting coefficients α are determined we can solve for $f(x)$ anywhere along the domain.

3. RBF INTERPOLATION OF SMOOTH AND DISCONTINUOUS FUNCTIONS

As discussed in previous sections, typically the shape parameter value c is chosen so that the interpolation matrix is approaching a high condition number close to ill-conditioned. This method tends to cause the error to decrease exponentially approaching spectral convergence. As this is an appropriate method for smooth functions it is not the case for regions of highly convective flows or steep gradients. It is actually the opposite as shape parameter values providing lower conditioning number for the interpolation matrix provides better results for steep gradients. This is shown in Fig. 2.

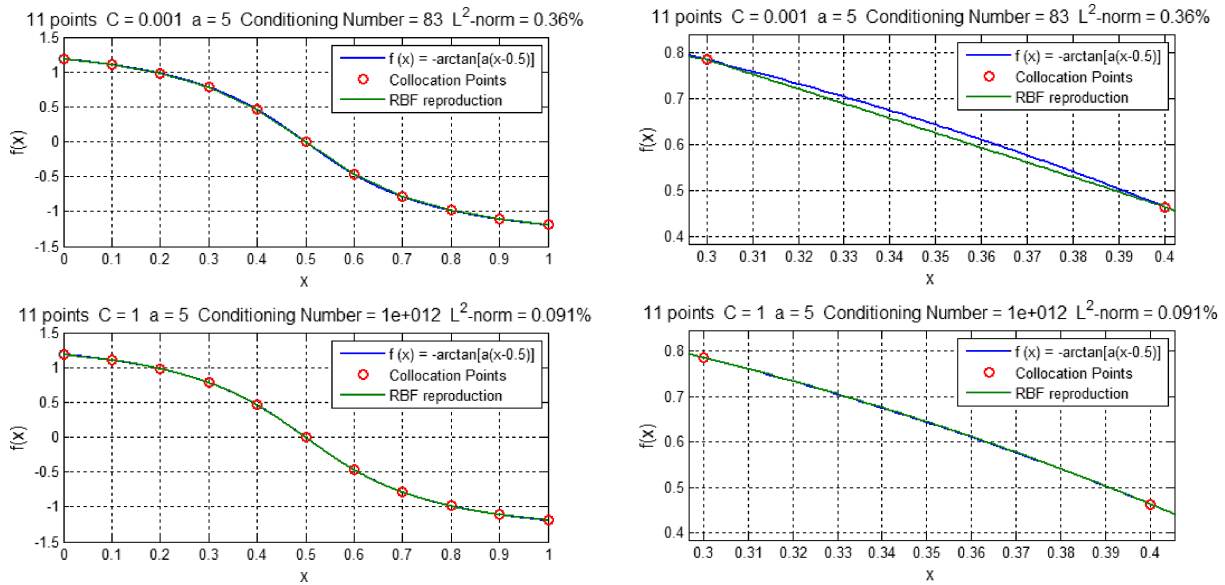


Fig. 2. Interpolation of smooth function using $c = 1$ and $c = 0.001$ for the test function $f(x) = -\arctan[a(x - 0.5)]$: test function and RBF reproduction (left) and zoomed-in plot (right).

As expected, the RBF does well at reproducing the smooth test function, but using a higher valued shape parameter gives a better result than the low value shape parameter. The RBF interpolation with a high shape parameter captures the curvature between collocation points better compared to the case with low shape parameter.

Next, to demonstrate the RBF interpolation on a discontinuity, a step function is chosen to be the test case. This is illustrated in Fig. 3.

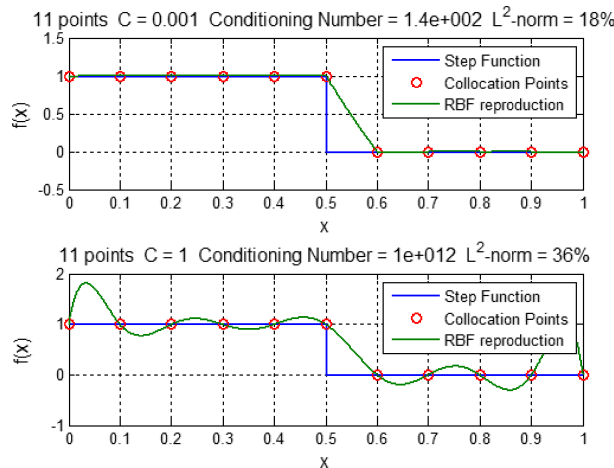


Fig. 3. Interpolation of step function using $c = 0.001$ and $c = 1$.

The RBF interpolation using a relatively large shape parameter of $c = 1$ and giving a conditioning number of $K = 1e + 12$ does not reproduce the test function. This is shown in the lower plot of Fig. 3. The RBF reproduction is oscillatory which researchers have discovered [4, 10]. However, for low valued shape parameters, the RBF interpolation does well in reproducing the test function.

To further demonstrate the effects of the shape parameter for smooth and discontinuous function interpolation, more examples are provided in Fig. 4 and Fig. 5. These figures present RBF interpolations of a test function and its derivatives, $f'(x)$ and $f''(x)$ for shape parameter values of $c = 0.1, 0.5,$ and 1.0 . Table 1 and Table 2 are supplement to the figures by tabulating the L^2 norm errors for $f(x)$ and $f'(x)$ and $f''(x)$ for the shape parameter values $c = 0.1, 0.5, 1.0$. Figure 6 is a plot of a 2-D surface with high gradients which is also supplemented by Table 3 showing the L^2 norm errors for $\frac{\partial f(x,y)}{\partial x}$, $\frac{\partial f(x,y)}{\partial y}$ and $\nabla^2 f(x,y)$.

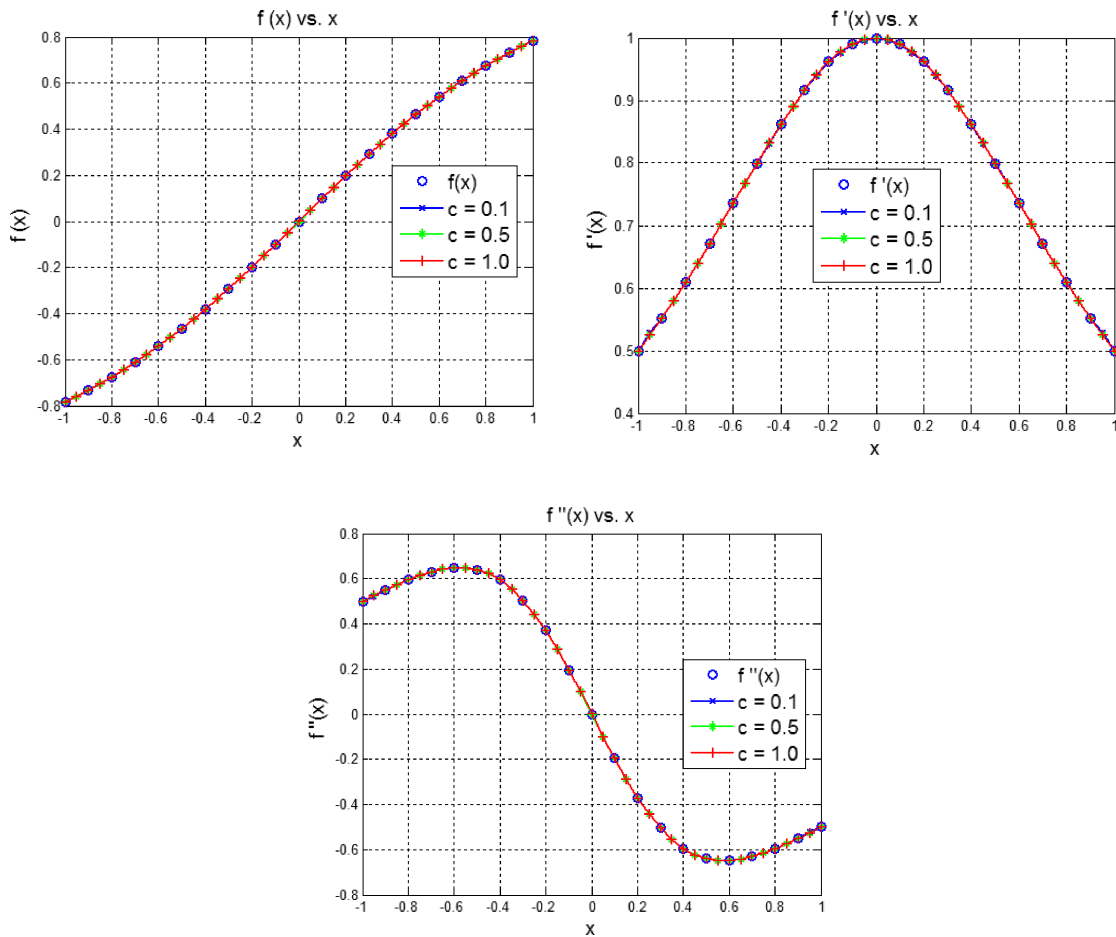


Fig. 4. Test function $f(x) = A \tan^{-1}[\omega(x - x_0)]$, $A = 1, \omega = 1$. Smooth function interpolation for $f(x), f'(x), f''(x)$.

Table 1. L^2 norms for smooth function RBF interpolation for Fig. 4.

c	$f(x)$	$f'(x)$	$f''(x)$
0.1	2.52e-4	0.0016	3.46e-4
0.5	3.20e-6	1.64e-5	5.71e-6
1.0	1.41e-8	4.41e-8	1.45e-8

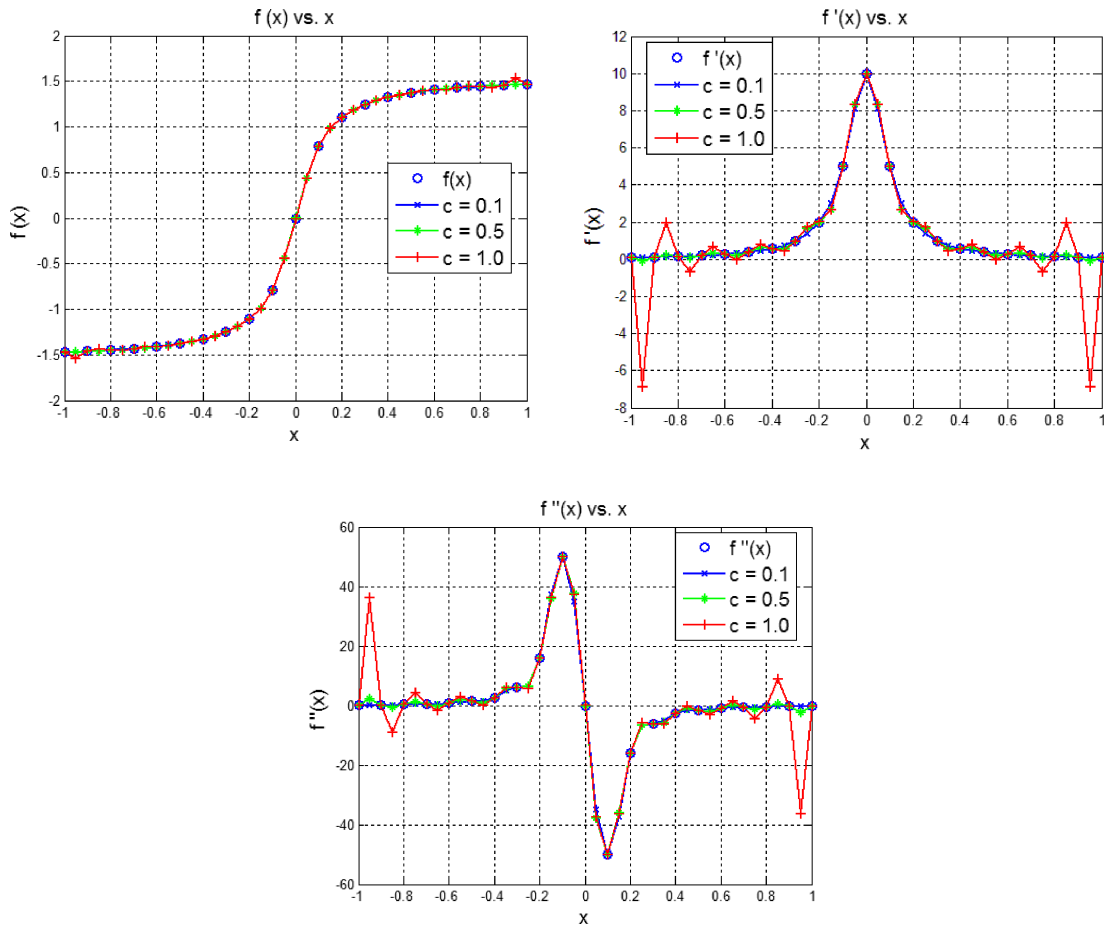


Fig. 5. Test function $f(x) = A \tan^{-1}[\omega(x - x_0)]$, $A = 1$, $\omega = 10$. Step gradient function interpolation for $f(x)$, $f'(x)$, $f''(x)$.

Table 2. L^2 norms for function with steep gradient RBF interpolation in Fig. 5.

c	$f(x)$	$f'(x)$	$f''(x)$
0.1	0.0021	0.0069	0.0526
0.5	0.0017	0.0167	0.0480
1.0	0.0060	0.2369	0.0810

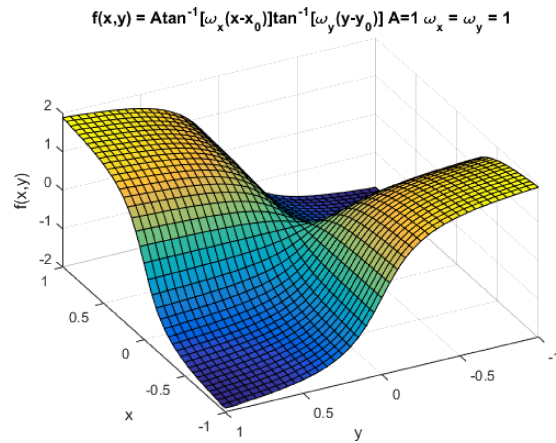


Fig. 6. 2-D RBF interpolation with steep gradients. Test function: $f(x,y) = A \tan^{-1}[\omega_x(x - x_0)] \tan^{-1}[\omega_y(y - y_0)]$.

Table 3. L^2 norms for function with steep gradient RBF interpolation in Fig. 6.

c	$f(x, y)$	$f_x(x, y)$	$f_y(x, y)$	$\nabla^2 f(x, y)$
0.1	0.0051	0.0522	0.0522	0.0964
0.5	0.0053	0.0436	0.0436	0.1363
1.0	0.0098	0.0437	0.0437	0.1763

4. RBF BLENDED INTERPOLATION APPROACH

To take advantage of the RBF interpolation when encountering both smooth and steep gradients in the field, the RBF interpolation scheme must have the capability to blend between high and low values shape parameter. The shape parameter, c , could be adjusted during the computation but a relationship for, c , is difficult to determine requiring time consuming numerical experimentation. A blended approach allows the user to set the shape parameter values for smooth and steep gradient interpolation and blend between the two interpolations as needed. We first assume the solution of the function $f_c(x)$ is in between the function $f_a(x)$ and $f_b(x)$ so that,

$$f_c(x) = f_a + \phi(f_b - f_a), \quad (7)$$

where f_a in this case is the smooth function interpolation, f_b is the steep gradient interpolation ϕ is the blending parameter, and f_c is the blended interpolation

$$f_a(x) = \sum_{j=1}^N \alpha_{a_j} \Psi_{a_j}(x), \quad (8)$$

$$f_b(x) = \sum_{j=1}^N \alpha_{b_j} \Psi_{b_j}(x). \quad (9)$$

Defining two RBF with high and low valued shape parameters c_a and c_b . The Hardy Multi-quadrics RBF is used as an example,

$$\Psi_{a_j}(x) = \sqrt{(x - x_j)^2 + c_a^2}, \quad (10)$$

$$\Psi_{b_j}(x) = \sqrt{(x - x_j)^2 + c_b^2}. \quad (11)$$

By introducing discrete points at locations x_i , the functions can be evaluated as

$$f_a(x_i) = \sum_{j=1}^N \alpha_{a_j} \Psi_{a_j}(x_i), \quad (12)$$

$$f_b(x_i) = \sum_{j=1}^N \alpha_{b_j} \Psi_{b_j}(x_i). \quad (13)$$

Next, the weights α_{a_j} and α_{b_j} must be determined. Equations (12) and (13) are used to form a system of equations using the scattered data of $f(x_i)$

$$[\Psi_a] \{\alpha_a\} = \{f\}, \quad (14)$$

$$[\Psi_b] \{\alpha_b\} = \{f\}. \quad (15)$$

Inverting the interpolation matrices $[\Psi_a]$ and $[\Psi_b]$ and solving for the weighting coefficients

$$\{\alpha_a\} = [\Psi_a]^{-1} \{f\}, \quad (16)$$

$$\{\alpha_b\} = [\Psi_b]^{-1} \{f\}. \quad (17)$$

Substituting Eqs. (16) and (17) into (7) we have the blended expression

$$f_c(x) = \sum_{j=1}^N \alpha_{a_j} \Psi_{a_j}(x) + \phi \left(\sum_{j=1}^N \alpha_{b_j} \Psi_{b_j}(x) - \sum_{j=1}^N \alpha_{a_j} \Psi_{a_j}(x) \right), \tag{18}$$

or in matrix form

$$f_c(x) = \{\Psi_a(x)\}^T [\Psi_a]^{-1} \{f\} + \phi \left(\{\Psi_b(x)\}^T [\Psi_b]^{-1} \{f\} - \{\Psi_a(x)\}^T [\Psi_a]^{-1} \{f\} \right), \tag{19}$$

$$f_c(x) = \left[\{\eta_a(x)\}^T + \phi \left(\{\eta_b(x)\}^T - \{\eta_a(x)\}^T \right) \right] \{f\}. \tag{20}$$

In the numerical examples to follow, the blending parameter is chosen to be either value of 0 or 1 to switch from high conditioning to low conditioning.

5. OVERVIEW OF RBF VIRTUAL POINT FINITE DIFFERENCE

The RBF virtual point finite difference uses the impressive capabilities of the RBF interpolation over scattered data points to create a virtual finite difference stencil. This method was developed to solve the stability issue with RBF interpolation when approximating the derivatives in regions where highly convective flow, steep gradients or discontinuities are present. By the creation of finite difference stencil, the well-developed upwind schemes, total variation diminishing (TVD) schemes, and limiters can be used. Figure 7 illustrates how the RBF virtual point finite difference is implemented.

This method is used with the RBF blended interpolation to further study the blended approach on model partial differential equations. The shape parameter is adapted to high or low value at each data center based on a criterion.

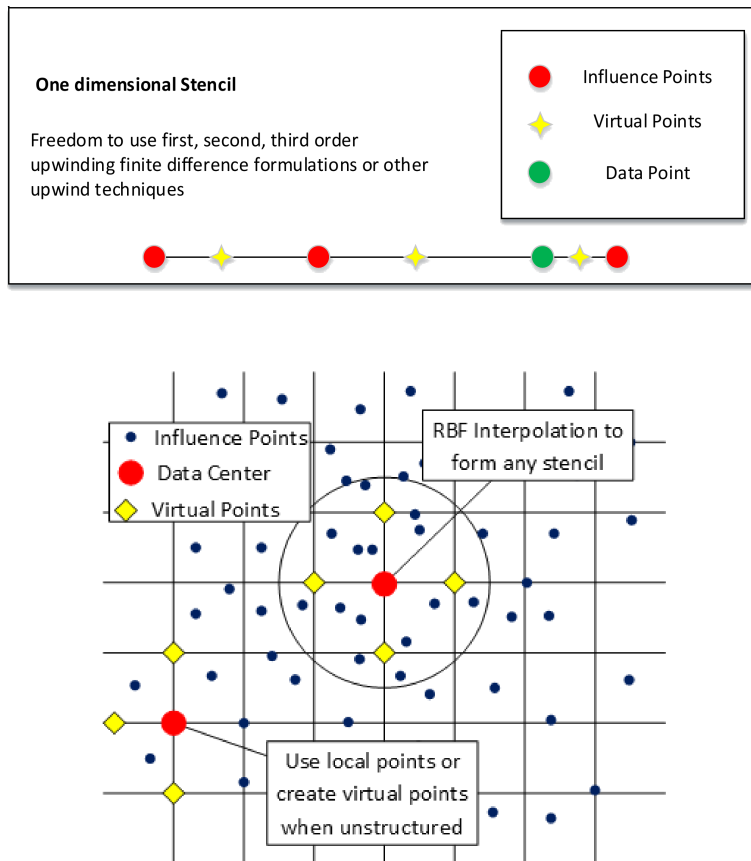


Fig. 7. Description of the RBF virtual point finite difference for one and two dimensions.

6. 1-D INVISCID BURGERS EQUATION

The solution of the 1-D inviscid Burgers equation is computed using the RBF blended approach and virtual finite difference. This example illustrates the blended interpolation concept applied to the solution of a PDE with a shock or discontinuity. The governing equation and the initial condition are

$$\frac{\partial u}{\partial t} + u \frac{\partial u}{\partial x} = 0, \quad u(x, 0) = 1 \quad \text{for } x < 0.5, \quad u(x, 0) = 0 \quad \text{for } x \geq 0.5. \quad (21)$$

The initial condition is shown in Fig. 8 as well as the collocation points which are chosen to be randomly distributed across the domain of $[0, 1]$ over x . The local collocation points are points $i+1$, i , and $i-1$, where i is the data center. These local collocation points are used for the RBF interpolation along the subdomain $[x_{i-1}, x_{i+1}]$. A distance Δx is used to interpolate for the value of u^n at $x_i - \Delta x$ to create an upwind stencil. With the upstream values of u^n known, a first order explicit scheme and first order or second order upwind finite difference in x is used at some constant distance Δx to calculate the next value of u at the next time step, u^{n+1} .

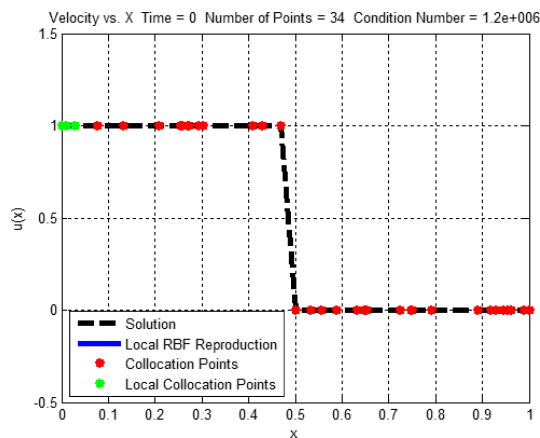


Fig. 8. Initial condition for the non-linear Burgers' equation solution.

To blend the RBF interpolation when a shock or steep gradient is present, a blending criterion is needed to determine when to adapt the shape parameter. It was hypothesized that the shape parameter is dependent on curvature of the field. This is observed in previous sections with the shape parameter dependency on the gradient as well as the shape parameter dependency on the number of collocation points used. An increase in number of collocation points can also reveal gradients and high curvature depending on the points location relative to one another. Therefore, a central difference of the second derivative is taken to be the metric to evaluate if the shape parameter must be changed. If the second derivative of the field variable is above some criterion to indicate steep gradients, the shape parameter is lowered else it remains high. Figures 9 and 10 describes this in further detail. In Fig. 9, the shape parameter is constant and set to a high value creating interpolation matrices with high conditioning, K . Recall that the high shape parameter and inherently the high condition number is ideal for smooth functions, but near steep gradient oscillations can appear. Figure 10 exhibits the case for the RBF blended interpolation. Relatively high shape parameter is used for the regions with low second derivative values indicated by the high conditioning numbers presented, but near the discontinuity the gradient is sense and the shape parameter is lowered. Note the conditioning number, K , when this occurs is approximately $K \sim 11$.

The solution to the inviscid non-linear Burgers equation is shown in Fig. 11 using the virtual finite differencing approach with support of the RBF blended interpolation. The collocation points in this example are randomly distributed. This solution illustrates the method eliminates oscillations allowing for a stable solution.

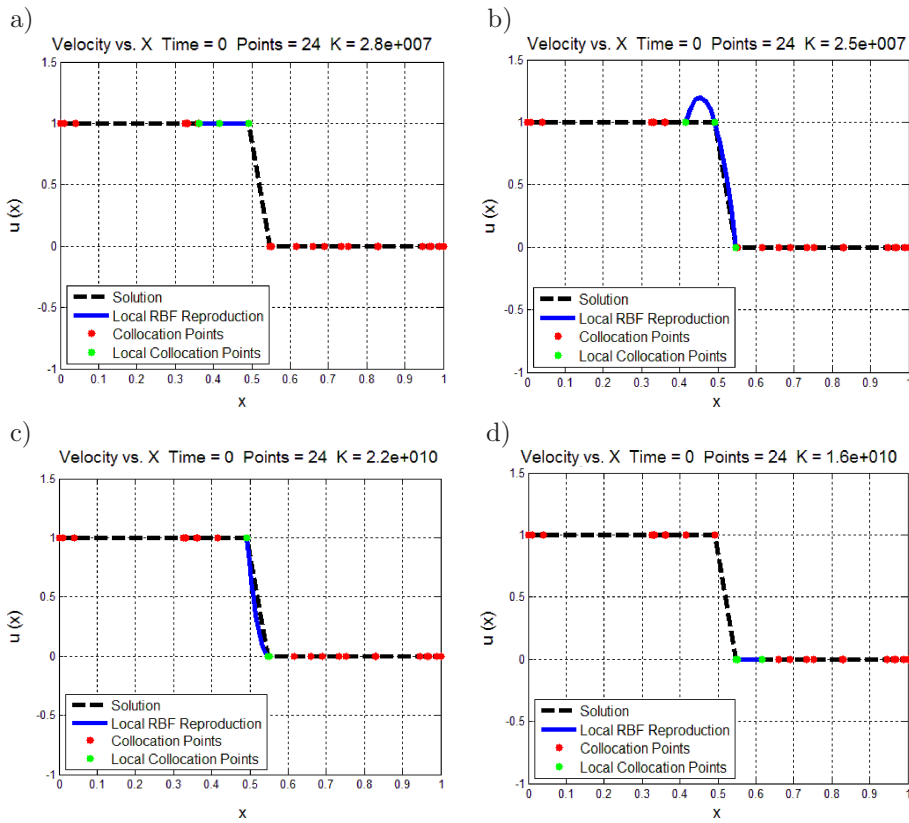


Fig. 9. Solution sweep with constant shape parameter interpolation approach: a) calculation before discontinuity $K = 2.8 \times 10^7$, b) at top of discontinuity $K = 2.5 \times 10^7$, c) at bottom of discontinuity $K = 2.2 \times 10^{10}$, d) after discontinuity $K = 1.6 \times 10^{10}$.

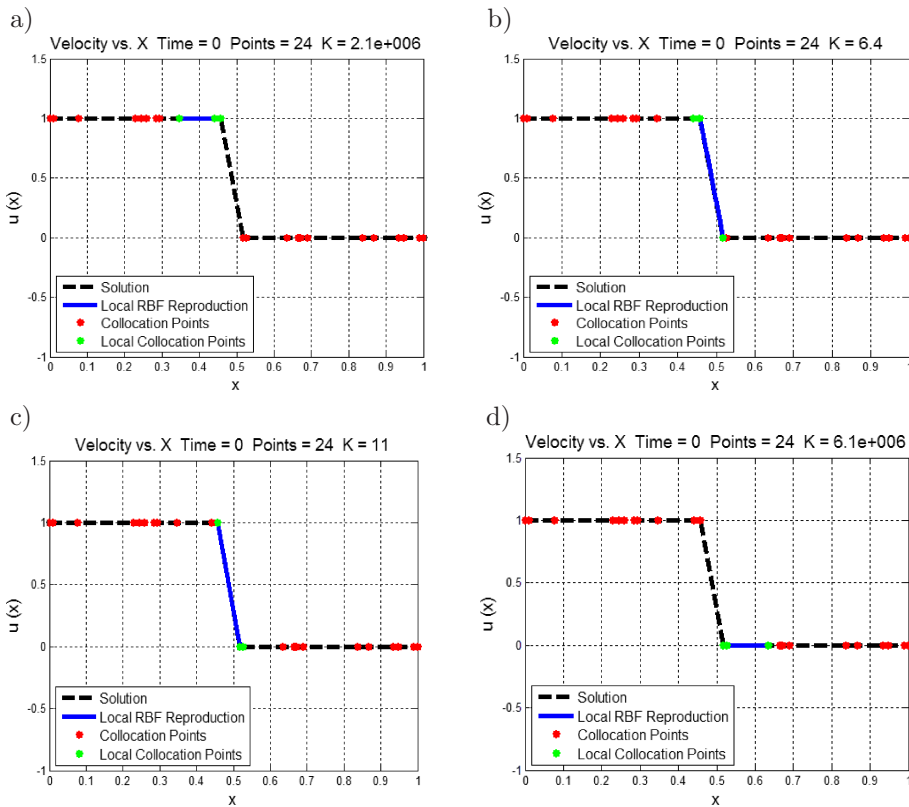


Fig. 10. Solution sweep with blended interpolation approach: a) calculation before discontinuity $K = 2.1 \times 10^6$, b) at top of discontinuity $K = 6.4$, c) at bottom of discontinuity $K = 11$, d) after discontinuity $K = 6.1 \times 10^6$.

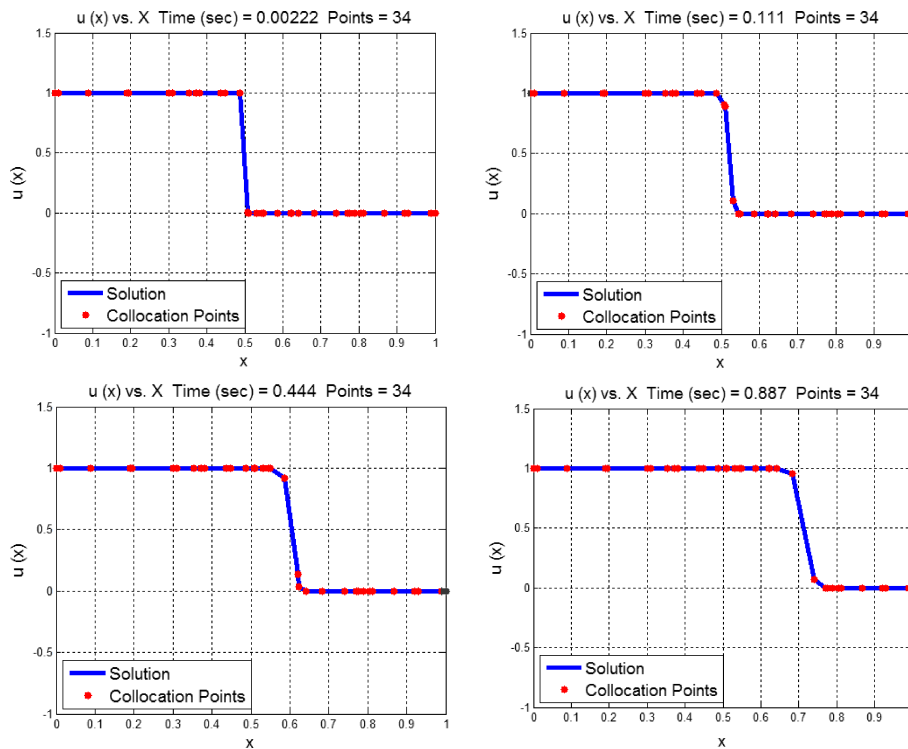


Fig. 11. Non-linear Burgers's equation solution using the RBF blending interpolation with the virtual point finite difference over a random distribution of points.

7. EXAMPLE: TWO DIMENSIONAL ADVECTION EQUATION

The two dimensional linear advection equation is solved using the RBF blended interpolation. A central differencing evaluating the Laplacian value using a high valued shape parameter RBF interpolation is used to determine when to adapt the shape parameter. If the Laplacian was above a predetermined criterion, then the shape parameter is lowered. Two cases are presented to demonstrate this approach. The first case is the 45° diagonally traveling wave which will be referred to as Case 1. The governing equation, boundary conditions and initial conditions for this case are

$$\frac{\partial u}{\partial t} + U_1 \frac{\partial u}{\partial x} + U_2 \frac{\partial u}{\partial y} = 0,$$

$$u(x, 0, t) = 2 \quad \text{for } x \leq 0.2,$$

$$u(x, 0, t) = 1 \quad \text{for } x \geq 0.2,$$

$$u(0, y, t) = 2 \quad \text{for } y \leq 0.2,$$

$$u(0, y, t) = 1 \quad \text{for } y \geq 0.2,$$

$$u(x, 0) = 0,$$

(22)

where

$$U_1 = \frac{\sqrt{2}}{2}, \quad U_2 = \frac{\sqrt{2}}{2}.$$

In Fig. 12, the solution to the case 1 is shown for constant shape parameter providing a high conditioning number for the interpolation matrix compared to a solution using the RBF blended

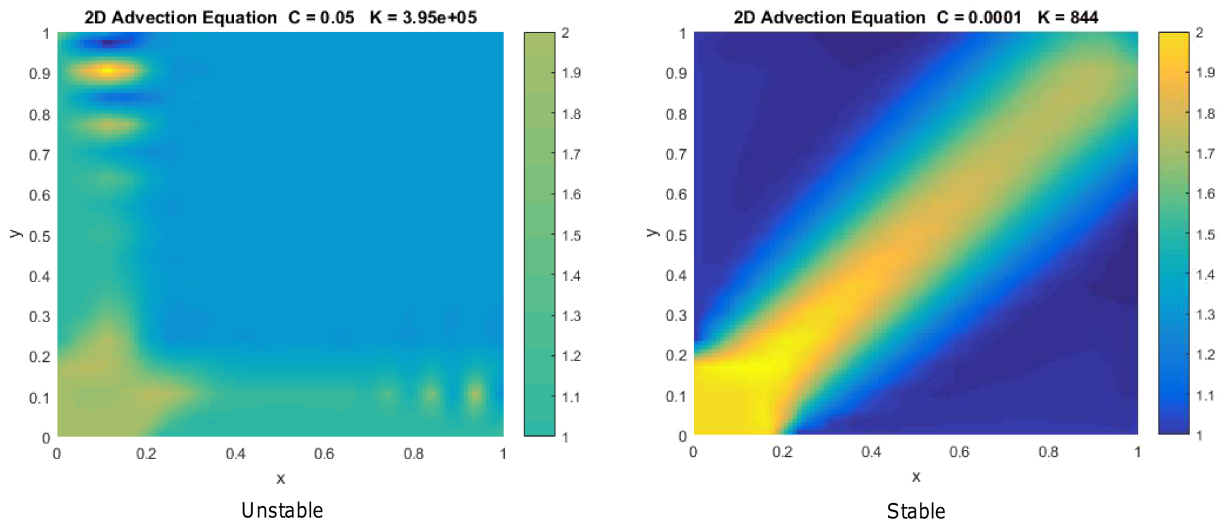


Fig. 12. Comparison of Case 1 with constant shape parameter with high condition number (left) to the RBF blended interpolation approach (right). Parameter c is the shape parameter and K is the conditioning number.

approach. The solution obtained using the constant shape parameter becomes oscillatory and unstable early in the simulation, while the blended shape parameter solution is stable.

The second case is the turning wave which will be referred to as Case 2. The governing equation, boundary conditions and initial conditions for this case are

$$\frac{\partial u}{\partial t} + U_1 \frac{\partial u}{\partial x} + U_2 \frac{\partial u}{\partial y} = 0, \tag{23}$$

where

$$U_1 = 2y[1 - (x - 1)^2], \quad U_2 = -2(x - 1)(1 - y^2).$$

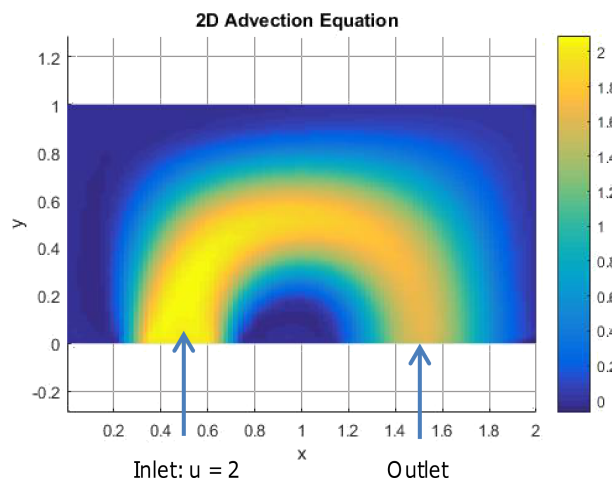


Fig. 13. Turning wave prescribed boundary conditions.

The solution of the turning wave is shown in Fig. 14. Again, for constant shape parameter and high conditioning number the solution eventually becomes oscillatory and unstable. Adapting the shape parameter, the solution remains stable.

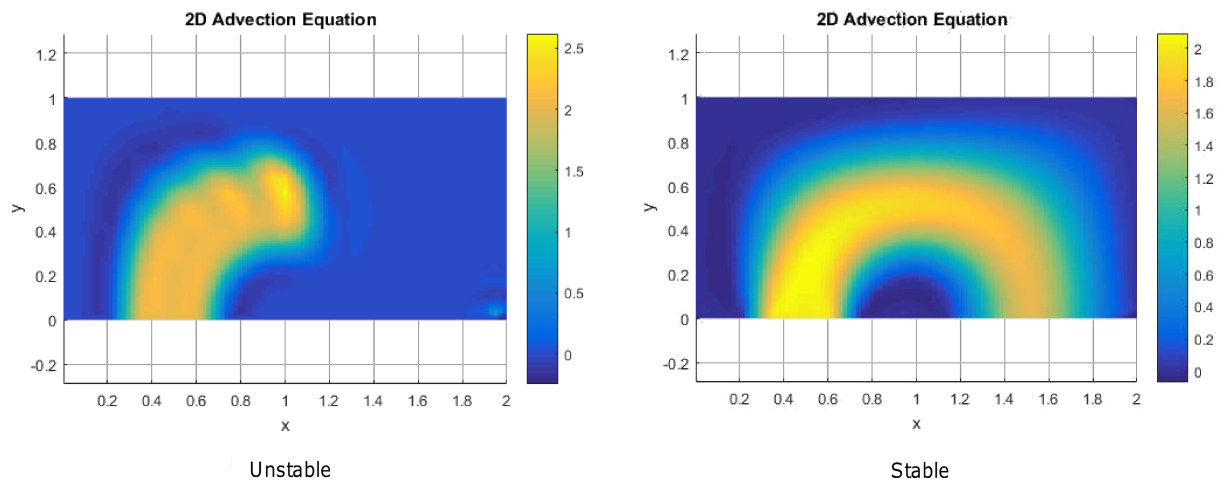


Fig. 14. Comparison of Case 2 with constant shape parameter with high condition number (left) to the RBF blended interpolation approach (right). Parameter c is the shape parameter and K is the conditioning number.

8. CONCLUSION

A method for the RBF interpolation of highly convective flow and steep gradients was presented in this paper. The blended RBF approach proposed the idea of blending the radial basis functions with different value shape parameters providing interpolations matrices with high and low conditioning numbers. Examples were presented describing the behavior of the RBF interpolation in the presence of steep gradients. In addition, the RBF Virtual Point Finite Differencing was used to solve the inviscid Burgers' equation and the two dimensional linear advection equation with support from the RBF blended interpolation. The RBF's were blended based on the curvature or second derivative of the field. If the curvature reached a specified criterion, representing high curvature, a low shape parameter and conditioning RBF interpolation was used. For future work, the blending parameter, ϕ , needs to be studied further to determine the criteria between smooth and steep gradient.

REFERENCES

- [1] A.H.-D. Cheng, M.A. Golberg, E.J. Kansa, G. Zammito. Exponential convergence and H-c multiquadric collocation method for partial differential equations. *Numer. Methods Partial Differ. Equ.*, **19**: 571–594, 2003.
- [2] B. Sarler, R. Vertnik. Local explicit radial basis function collocation method for diffusion problems. *Comput. Math. Appl.*, **51**(8): 1269–1282, 2005.
- [3] B. Sarler, T. Tran-Cong, C.S. Chen. Meshfree direct and indirect local radial basis function collocation formulations for transport phenomena. *Boundary Elements XVII*, A. Kassab, C.A. Brebbia, E. Divo [Eds.], WIT Press, Southampton, UK, pp. 417–428, 2005.
- [4] S. Gerace, K. Erhart, A. Kassab, E. Divo. A model-integrated localized collocation meshless method for large scale three dimensional heat transfer problems. *Engineering Analysis*, **45**: 2–19, 2014.
- [5] J. Kelly, E. Divo, A.J. Kassab. Numerical Solution of the Two-Phase Incompressible Navier-Stokes Equations using a GPU-Accelerated Meshless Method Engineering Analysis with Boundary Elements. *Engineering Analysis*, **40C**: 36–49, 2014.
- [6] S. Gerace, K. Erhart, E. Divo, A. Kassab. Adaptively refined hybrid FDM/meshless scheme with applications to laminar and turbulent flows. *CMES: Computer Modeling in Engineering and Science*, **81**(1): 35–68, 2011.
- [7] K. Erhart, A.J. Kassab, E. Divo. An inverse localized meshless technique for the determination of non-linear heat generation rates in living tissues. *International Journal of Heat and Fluid Flow*, **18**(3): 401–414, 2008.
- [8] E.A. Divo, A.J. Kassab. An efficient localized RBF meshless method for fluid flow and conjugate heat transfer. *ASME Journal of Heat Transfer*, **129**: 124–136, 2007.
- [9] E.A. Divo, A.J. Kassab. Iterative domain decomposition meshless method modeling of incompressible flows and conjugate heat transfer. *Engineering Analysis*, **30**(6): 465–478, 2006.
- [10] E. Divo, A.J. Kassab. Localized meshless modeling of natural convective viscous flows. *Numerical Heat Transfer, Part B: Fundamentals*, **53**: 487–509, 2008.